International Journal of Rail Transportation

ISSN: 2324-8378 (Print) 2324-8386 (Online) Journal homepage: www.tandfonline.com/journals/tjrt20

Railway capacity analysis: impact of platooning under modular pods operations

Zheng Ning, Egidio Quaglietta & Mahnam Saeednia

To cite this article: Zheng Ning, Egidio Quaglietta & Mahnam Saeednia (25 Feb 2026): Railway capacity analysis: impact of platooning under modular pods operations, International Journal of Rail Transportation, DOI: 10.1080/23248378.2026.2631501

To link to this article: https://doi.org/10.1080/23248378.2026.2631501

Published online: 25 Feb 2026.

INTERNATIONAL JOURNAL OF RAIL TRANSPORTATION
https://doi.org/10.1080/23248378.2026.2631501

Taylor & Francis
Taylor & Francis Group

Railway capacity analysis: impact of platooning under modular pods operations

Zheng Ning, Egidio Quaglietta and Mahnam Saeednia

Department of Transport and Planning, Delft University of Technology, Delft, The Netherlands

ABSTRACT

Rail pods are an emerging concept of modular self-propelled rail vehicles which can interchangeably move freight and passengers to provide a more customer-oriented rail service. Pods are envisaged to operate on demand with the possibility of forming platoons either physically (e.g. mechanical or digital couplers) or virtually (e.g. by radio communication) coupling at stations. This study addresses the need to understand how rail pod platoons affect rail corridor capacity by analysing the actual infrastructure occupation under different platoon compositions, taking into account train movement dynamics and signalling constraints. First, this study extends the consolidated rail capacity assessment method (UIC Code 406) by applying the blocking time theory to assess the infrastructure occupation of the rail pod platoons. Based on this extension, a nonlinear optimization model is developed to determine coordinated speed profiles that are structurally consistent with the platoon configuration, aiming to minimize rail capacity utilization. The model is applied to a case study considering the ETCS Level 2 signalling system. The results obtained for the case study illustrate the ability of the proposed model to identify operational speeds and composition of rail pod' platoons that lead to the effective capacity use of the existing infrastructure. This capacity assessment framework provides a theoretical foundation for flexible allocation of modular rail cars in dynamically structured platoons.

ARTICLE HISTORY
Received 23 September 2025
Revised 9 February 2026
Accepted 9 February 2026

KEYWORDS
Capacity evaluation; Pods4Rail; modular rail platoons; coordinated speed configuration; dynamic headway constraints

1. Introduction

Delivering customer-oriented rail services requires greater system flexibility and seamless operations, prompting the development of innovative operational paradigms. Pods4Rail l [1,2], an EU-funded project developing a next-generation modular and intelligent rail system, introduces autonomously driven, reconfigurable self-propelled rail cars (pods) which can interchangeably move freight and passengers for a more flexible rail service. On-demand rail pod services may operate without a fixed timetable and follow a dynamic schedule to adapt to changes within-day of the customer demand. However, effective adaptation requires a precise quantification of the

CONTACT Zheng Ning Z.Ning@tudelft.nl Department of Transport and Planning, Delft University of Technology, Delft, The Netherlands

This article was originally published with errors, which have now been corrected in the online version. Please see Correction (http://dx.doi.org/10.1080/23248378.2026.2646810)

system's usable capacity. This defines the maximum operable supply, enabling dispatching decisions to determine the 'available capacity' within any time window to match fluctuating demand. Nevertheless, similar to conventional trains, rail pods must maintain safe separation from other vehicles in compliance with signalling constraints, ensuring conflict-free operations.

Notably, the temporal overlap of origin-destination pairs among pod transport tasks within shared track sections creates operational windows for forming platoons. Operating on existing infrastructure, pods are designed to travel independently or dynamically form platoons by coupling at key locations such as stations or junctions. Coupling can be implemented either physically (using mechanical or digital couplers) or virtually (e.g. via radio communication). This dynamic coupling and decoupling mechanism enables pods to reconfigure their platoon compositions by adjusting the platoon size and headway in response to fluctuating transport demand and rolling stock performances (e.g. braking/acceleration rates) in compliance with signalling constraints [3–5]. This structural flexibility supports demand-adaptive operations and contributes to improved system efficiency (for more details, see [6]).

As a modular transport system, pods require coordinated operations to respond to dynamic transport demand. Recent research has begun to address the associated scheduling challenges by proposing optimization frameworks specifically tailored to rail pod systems. A simulation-based framework for evaluating the impact of dispatch and platooning decisions on system performance is presented in [7], and the results show that platooning can significantly reduce makespan in large-scale operational scenarios. Based on this [8], proposes a freight service planning model formulated as a Pickup and Delivery Multi-Depot Vehicle Routing Problem (PDMVRP) with integrated platooning strategies. The main limitation of the proposed approaches is that they identify demand-driven pod platoon schedules while neglecting the safety-related signalling constraints which actually dictate the feasibility of a given schedule.

Considering the actual infrastructure and signalling constraints is hence essential to determine the feasibility of given rail pod schedules and the corresponding operational impacts. Several challenges still exist in assessing the capacity of rail infrastructure when rail pod platoons are operated, because this depends on multiple factors such as platoon formation, cruising speed, pod braking performance, and signalling system type. Standard capacity evaluation frameworks, including UIC Code 406 [9], simplify system characteristics by assuming fixed cruising speeds and uniform headways, thereby reducing computational complexity and enabling broader applicability. However, enabling demand-responsive operations in the pod system requires flexible formation and reconfiguration of platoons composed of modular vehicles. Ignoring variation in block occupation times associated with different platoon lengths can lead to either an underestimation of conflict risks due to short headways or inefficient capacity utilization due to overly conservative spacing. Consequently, these models cannot accurately capture the actual capacity implications of the deployment of pods within existing railway systems.

This study addresses this gap by proposing a capacity evaluation model for pod platoons with variable formations (i.e., platoons with different sizes composed of pods with homogeneous characteristics), which accounts for non-uniform headways between platoons and optimizes infrastructure occupancy through coordinated platoon speed.

This approach considers platoons composed of homogeneous pod units, arranged in varying platoon formations. The main contributions of this research are:

- Extending the UIC 406 methodology with blocking time theory to support the implementation and adaptation of the modular pods system on existing railway infrastructure.
- Establish a foundational capacity assessment model that incorporates signalling rules, spatial separation, coordinated speed profiles, and platoon structures into the evaluation process.
- Evaluated under the ETCS Level 2 signalling system, the proposed model offers quantitative support for scheduling and traffic management decisions.

The paper is organized as follows. Section 2 reviews the related literature. Section 3 extends blocking time theory and the UIC 406 capacity model to establish a capacity occupancy model for pod platoons, serving as a dynamic headway constraint. Based on this extension, a nonlinear optimization model is developed to determine the optimal coordinated cruising speeds of platoons, aiming to minimize infrastructure occupation while ensuring safety margins. The simulation results are analysed in Section 4. Section 5 concludes the paper.

2. Literature review

2.1. Application overview of modular rail pods system

A pod vehicle comprises two core components (shown in Figure 1): Transportation Units (TUs) and Carriers Units (CUs). TUs function as demand-driven, modular loading entities enabling automated and rapid decoupling from and recoupling with CUs, supporting the seamless transfer of loaded TUs across multi-modal transport networks, including road and rail. CUs act as mobile service terminals, with their dispatching strategies adhering to the spatio-temporal pickup and delivery requirements of the TUs. Upon assembly at designated operating stations, the TUs and a carrier form a complete pod. A pod serves as the fundamental operational entity on the rail tracks, regardless of

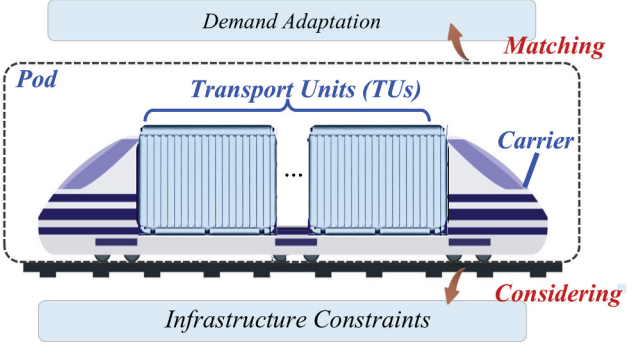

Figure 1. Pods architecture with transportation units (TUs) and carriers.

whether the carrier is transporting TUs or running empty. An empty carrier moving along the rail line is still regarded as an individual pod.

Key technological innovations, such as Virtual Coupling (VC) [10–12] and digital automatic coupling (DAC) [13], are driving the transition from fixed train to flexible platooning. VC enables the close follow-up of trains via wireless communication, potentially increasing capacity [14,15], while DAC facilitates dynamic formation configuration through mechanical links and distributed control. The relationship between capacity and convoy structure in VC systems is investigated in [16]. The results show that with an optimized convoy composition aligned with infrastructure and service requirements, a VC platoon can increase infrastructure utilization by up to 30%. These technologies provide the conditions for the platoon operation of pods.

Modular rail pod deployment, with the aim of improving infrastructure utilization and operational efficiency, remains an emerging concept, and research in the field, related to the impact on infrastructure, remains limited. Originally developed in the context of modular vehicle-based road transit systems, this technology is now being introduced into the railway system [17]. Modular vehicles have attracted increasing attention in public transport research due to their ability to dynamically adjust the length of movement entities by coupling or decoupling vehicles in response to fluctuating demand [18]. Most existing studies primarily focus on planning-level scheduling problems, with the objective of optimizing tasks assignment to satisfy the demand for pickup and delivery. A platoon scheduling and speed optimization model for a bus network, which reduces both operator and passenger costs along a single bus line, is presented in [19]. Broader research within the modular vehicle framework has explored various optimization problems, including vehicle routing [20–22], platoon formation and time scheduling [22,23], as well as the integration problem of passenger and freight operations [24,25]. When integrated with existing infrastructure, these studies typically rely on the assumption that sufficient capacity is available or that the range of usable capacity can be clearly defined. However, under speed and separation constraints, the infrastructure occupancy of modular trains becomes complex and is not adequately captured by simplified modelling assumptions.

2.2. Review on rail capacity assessment

Railway capacity is inherently dynamic, influenced by train operational performance, signalling system, infrastructure layout, and scheduling/dispatching strategies [9]. UIC Code 406, formally adopted as a static capacity evaluation standard in European railways, defines a methodology based on compressing existing timetables within a defined time window [26]. Fundamentally, the approach determines the minimum feasible time separation between consecutive trains, representing the safety headway required under given train dynamics and signalling response characteristics, as defined by the blocking time theory. The blocking time model computes the total time that a given portion of railway infrastructure is exclusively allocated to a train from the time it reserves the route until the train clears it with its whole length, and the signalling resets that to a vacant state (so-called ‘track release’).

Figure 2 illustrates the blocking time composition for trains operating on line sections, both with and without scheduled station stops. Regardless of whether a train is scheduled

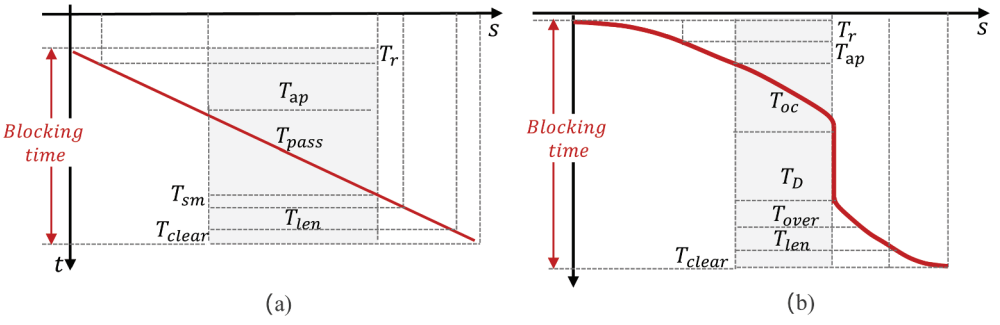

Figure 2. Diagram of the composition of the blocking time: (a) the inter station segment blocking time for a train, (b) the station segment blocking time for a train.

to stop, the pre-blocking time remains unchanged, consisting of the route setting time T_{r}, approach time T_{ap}, and track occupation time T_{pass}. In the non-stopping case, the signal is released after the train's rear clears both the block section and the safety margin, resulting in the clearance time T_{clear} and the safety margin time T_{sm}. In contrast, when a scheduled stop is made, the station dwell time T_{D} is added, and the signal can only be released after the train's rear clears the overlap section leading to the overlap time T_{over}.

The UIC 406 capacity evaluation is a consolidated method; however, it relies on an existing timetable and mostly applies to corridors rather than complex rail configurations, such as double-line junctions. Another main limitation is that this is applicable to existing rail operational paradigms, which are typically based on fixed operational patterns, such as consistent train types and uniform speed strategies. Although modular rail pods are designed to move synchronously in a platoon, braking distance constraints should still be considered to maintain safe separation. However, conventional capacity evaluation paradigms often do not include advanced operational concepts such as modular pods and platooning. These methods inevitably overlook operational variability, such as changes in train speeds, train formations, and stochastic disturbances or delays [27–30]. To address these limitations, several complementary approaches have been proposed, including simulation-based methods such as the Federal Railroad Administration (FRA) capacity model [31] and model-based optimization frameworks [32,33]. While simulation models reflect real-world railway operations more accurately, they are often limited to specific scenarios, whereas optimization-based methods broaden the analytical scope by abstracting train dynamics and scheduling logic into mathematical models. However, such models still typically depend on predefined parameters, such as minimum headways and speed profiles, limiting their adaptability to dynamic operating conditions.

Some studies have explored extensions of the UIC 406 capacity model, in order to improve its applicability to more complex operational scenarios. A comparison of Indonesian and Japanese methods for rail capacity, including variable definitions and policy implications, is provided in [28]. The flexible rail service concept, which does not follow a fixed timetable, has been proposed to schedule train operations by means of techniques such as reinforcement Learning [34,35] to schedule train operations. A distributed moving-block approach for train sequencing, using

Table 1. Summary of related studies versus the proposed framework.

Study	Formation	Timetable	Speed	Methodology	Output/Focus
Conventional Capacity Assessment					
UIC 406 [9]	Fixed	✓ (Required)	Uniform	Timetable Compression	Static Capacity
Landex [27]	Fixed	✓ (Required)	Uniform	UIC 406 Extension	Network Evaluation.
Sameni [30]	Fixed	✓ (Required)	Uniform	Blocking Time.	Junction Capacity
Bešinović [29]	Fixed	✓ (Optimized)	Dynamic	Microscopic Simulation	Integrated Planning
Widyastuti [28]	Fixed	✓ (Required)	Uniform	Comparative Analysis	Policy Implications
Modular Vehicle Routing					
Chen & Li [17]	Variable	× (Demand)	Fixed	Discrete Modelling	Station Docking
Tian [19]	Variable	× (Demand)	Optimized	Joint Scheduling Model	Operation Costs
Fu & Chow [23]	Variable	× (Demand)	Fixed	Dial-a-ride Problem	En-route Transfers
Liao [7]	Variable	× (Dynamic)	Fixed	Heuristic Framework	Pods Scheduling
Zhou [22]	Variable	× (Demand)	Fixed	Vehicle Routing	Logistics Routing
Flexible/Virtual Coupling Operations					
Khadilkar [35]	Fixed	× (Required)	Dynamic	Reinforcement Learning	Dispatching Policy
Quaglietta [11]	Fixed	/	Dynamic	State Machine Model	VC Dynamics
Ning [16]	Variable	✓ (Adjust)	Coordinated.	Coalition Game	Convoy Structure
Wu [12]	Variable	✓ (Optimized)	Coordinated	MILP Optimization	Heavy Haul.
This Study	Variable	× (On-demand)	Coordinated	Blocking Time + NLP	Capacity

simulated block occupancy logic for safety, is proposed in [36]. Existing railway capacity assessment methods are not directly applicable to rail pod platoons, because the platoon length varies with the number of pods and requires maintaining safe braking distances even under synchronous movement. Existing static metrics such as 'trains per hour' are not suitable to evaluate the capacity of systems with dynamically coupled units.

A comparative overview of these studies is presented in Table 1, which maps out the differences in formation flexibility and methodological limitations.

As evident in Table 1, while existing research has explored conceptual architecture and demand-driven scheduling for pod systems, significant gaps remain in capacity modelling and infrastructure evaluation. The research in this paper addresses critical knowledge gaps by examining how platoon structures and coordinated cruising speeds influence capacity consumption under fixed-block and radio-based signalling systems with dynamic speed supervision, such as ETCS Level 2 signalling system [37,38]. In particular, it investigates the effects of parameter variations (e.g., changes in platoon length) and the integration of these unique pod features with existing infrastructure while ensuring safe headway separation.

3. Methodology

This section develops a quantitative model to evaluate infrastructure capacity under modular pod configurations of variable platoon structure. It begins with the problem formulation and modelling assumptions in Section 3.1. Section 3.2 outlines the modelling framework and defines notations. Section 3.3 applies a spatial discretization approach to simulate train movements and formulates a running time computation model. Section 3.4 extends the UIC 406 blocking time model to calculate dynamic headway constraints based on platoon composition. Section 3.5 formulates an optimization model to minimize infrastructure occupation by coordinating the cruising speeds of multiple platoons.

3.1. Problem description and assumptions

Rail corridors equipped with the pods system need to accommodate multiple size platoons, each capable of dynamically adjusting its length through coupling and decoupling operations. As shown in Figure 3, each block may have an optimal speed that locally minimizes blocking time for a given platoon configuration. However, ensuring continuity in the speed profile across the blocks between two stations requires applying a unified cruising speed. Simultaneously, the blocking time induced by the optimal speed profiles under different platoon lengths affects the occupation of shared track resources, which further complicates capacity management. This interdependence gives rise to an optimization problem that coordinates the cruising profiles of multiple platoons to quantify capacity by minimizing infrastructure occupation.

Let $\mathcal{P} = \{P_1, P_2, \ldots, P_N\}$ denote the set of rail pod platoons to be dispatched in response to a specific set of demand request. The rail pod system is characterized by the following features:

- Formation type: A group of pods can be partitioned into different platoon structures, ranging from individual units to short or long platoons, each managed under a unified control envelope. These structural configurations determine key operational parameters and directly influence the infrastructure occupation. In particular, even with the same number of pods, alternative partitioning schemes can result in different platoon structures (e.g., splitting six pods into formations 2–2–2 or 3–1–2), thereby affecting capacity usage. In this study, *platoon structure* refers to the overall grouping of multiple pods into one or more platoons, while *platoon composition* is used to describe the internal configuration of a platoon, such as the number of pods and their sequence.
- Speed profile conditions: The motion of each platoon between two stations must comply with a predefined speed profile, typically comprising acceleration, cruising, and braking phases, dictated by section speed limits and train performance constraints. This profile ensures safe operation under signalling and infrastructure limitations while enabling consistent integration with scheduling frameworks.
- Global coordination speed optimization among platoons: Due to the interdependent nature of platoons of different sizes, determining coordinated cruising speeds becomes essential for optimizing the overall infrastructure utilization. Specifically, for a given platoon structure, the cruising speeds of multiple platoons must be

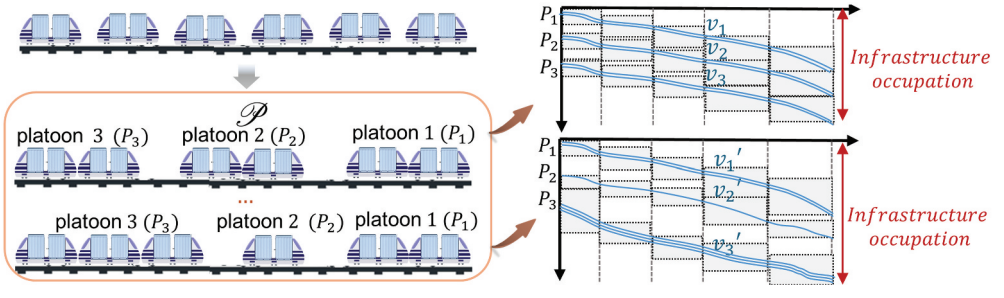

Figure 3. Block occupancy diagram for pod platoon traffic with different sizes.

jointly determined to minimize block occupancy across multiple blocks, rather than assigning each platoon its own locally optimal speed.

The proposed framework operates under these fundamental assumptions, aligned with the railway signalling system specifications.

- Constant acceleration (a_{tra}) and deceleration (a_{bra}) rates are assumed to represent the operational rates of homogeneous pod units on the fixed line [4,38]. This assumption allows nominal pod infrastructure occupation times to be evaluated while implicitly accounting for physical factors such as variable gradients and resistance.
- All pod units are assumed to be homogeneous with identical dynamic characteristics. This assumption enables a focused investigation of how platoon formation and speed coordination affect infrastructure occupation.
- The platoon composition is assumed to remain static during operation, with a fixed number of pods assigned to each platoon, as structural changes are only permitted at stations.
- All rail pods within a platoon are assumed to respond synchronously to control commands, functioning as a unit. This operational consistency can be achieved through virtual coupling via synchronized control method or physical coupling mechanisms.

3.2. Modelling framework and notions

As illustrated in Figure 4, the proposed modelling framework takes three categories of input data, drawn from infrastructure, vehicle characteristics, and transport demand. This framework is structured as a mathematical optimization problem, defined by three fundamental components shown in orange. The optimization module comprises two interdependent intermediate modules, highlighted in blue, which compute the necessary intermediate values used to evaluate the objective and constraints. The running time computation module first calculates the time required to pass through each block, a value that is directly affected by the cruising speed of each pod platoon. These times are then

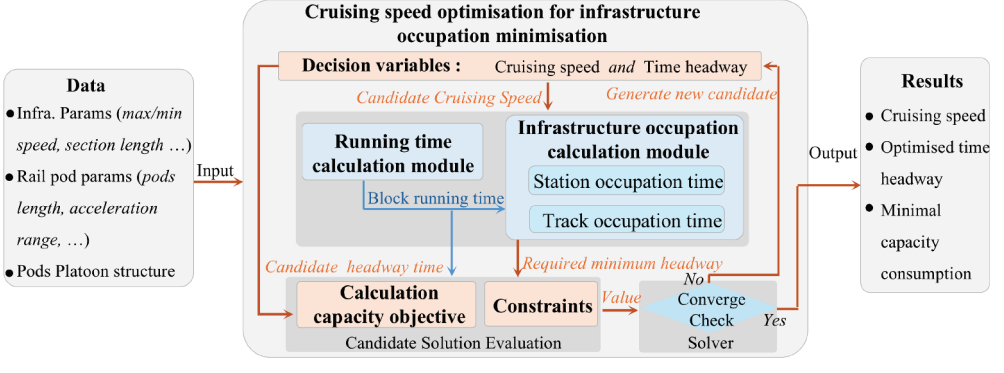

Figure 4. Quantitative capacity evaluation modelling framework for modular pods.

used as input to the infrastructure occupation evaluation module. The resulting occupation times serve a dual purpose, providing the primary inputs for the objective function's calculation, while also being fed back as dynamic headway constraints.

The iterative loop in Figure 4 is driven by a solver which, in each iteration, proposes a candidate solution for evaluation. Subsequently, the Converge Check module determines whether the process should terminate. This process is repeated iteratively until the solver converges on an optimal solution, which is then output. The infrastructure occupation model extends the blocking time theory to accommodate variable platoon structures, while the speed profiles are constrained to conform to the operational properties of railway systems. The detailed mathematical formulation of these models is presented in the subsequent sections, with the iterative loop logic and its candidate-variable solution update strategy described in Section 3.5.2 and Table 3.

The mathematical notation used in this paper is formally defined in Table 2.

Table 2. Symbol definitions.

Symbol	Definition	Unit
Parameters		
$\mathcal{I}$	Set of platoon indices, where $\mathcal{I} = \{1, 2, \ldots, N\}$	–
$\mathcal{J}$	Set of block indices, where $\mathcal{J} = \{1, 2, \ldots, M\}$	–
N	Total number of platoons	–
M	Total number of blocks	–
ζ	Number of discretized control segments under MBS	–
n_i	Number of pods in platoon i	–
a_j	Block type indicator (0: station, 1: interstation track)	–
ε	Small positive constant for numerical stability	–
S	Total distance between two stations	m
Δs_j	Length of generalized discrete segment j	m
l_j	Length of block section j	m
L_r	Distance travelled during reaction time	m
L_{bra}	Braking distance	m
L_j^{total}	Distance from departure station to start of block j	m
L_{pla}	Platform length	m
L_{over}	Platform protection section length	m
$L_{sta,de}$	Distance to station approach boundary	m
L_{sm}	Safety margin	m
L_c	Distance travelled after signal clearance	m
L_{lenP}	Pod vehicle length	m
S_{intra}	Intra-platoon safety spacing	m
$\Delta s_{req}^{(i,j)}$	Remaining acceleration or braking distance of platoon i in block j	m
$v_{i,j}^{in}$	Entry speed of platoon i at block j	m/s
$v_{i,j}^{out}$	Exit speed of platoon i at block j	m/s
v_i^{cru}	Cruising speed of platoon i	m/s
v_{sta}	Station speed limit	m/s
v_{min}	Minimum reference speed for braking calculation	m/s
V_{crit}	Critical velocity for acceleration profile	m/s
a_{tra}	Maximum traction acceleration	m/s^2
a_{bra}	Maximum braking deceleration	m/s^2
$a_{i,j}$	Acceleration of platoon i in block j	m/s^2
T_r	Train reaction time	s
T_{clear}	Block clearance time	s
T_D	Platform dwell time	s
T_{ap}	Approach braking time	s
T_{pass}	Block traversal time	s
T_{sm}	Safety margin time	s
T_{len}	Platoon length traversal time	s

(*Continued*)

Table 2. (Continued).

Symbol	Definition	Unit
T_{over}	Platform protection traversal time	s
$T^{\text{line}}(n)$	Line blocking time of an n-pod platoon	s
$T^{\text{sta}}(n)$	Station blocking time of an n-pod platoon	s
$t_{i,j}$	Time when platoon i clears block j	s
$T_{i,j}^{\text{pass}}$	Traversal time of platoon i in block j	s
$\Delta T_{i,j}$	Running time over discrete segment j	s
$H_{\min}$	Minimum allowable headway	s
δ_v	Velocity tolerance threshold	m/s
x	Decision variable vector (cruising speeds and headways)	–
μ, ρ	Barrier and penalty parameters	–
$\mathcal{K}$	Set of inequality constraint indices	–
$c_k(x)$	k-th inequality constraint function	–
H	Hessian matrix of the optimization problem	–
d, η	Search direction and step size	–
Decision Variables		
v_i^{cru}	Optimized cruising speed of platoon i	m/s
$h_{\text{opt}}^{(i-1,j)}$	Recommended headway between platoons $i-1$ and i in block j	s

3.3. Pods' running time formulation

The running time $T_{i,j}^{\text{pass}}$ of the platoon i through the block j plays a critical role in evaluating infrastructure capacity, particularly under different platoon structures in the pod system. Here, $i \in \mathcal{I} = \{1, \ldots, N\}$ and $j \in \mathcal{J} = \{1, \ldots, M\}$ refer to the platoon and block indices, respectively. This running time must be computed according to the speed profiles imposed by the infrastructure and signalling system, as illustrated in Figure 5, which reflects segment-specific speed limits and operating rules.

Discrete modelling of train movements along railway segments is a widely adopted approach in railway operations research to simulate the train operation process [39–43]. To accurately compute $T_{i,j}^{\text{pass}}$, the railway line is discretized into control segments. The total length S of the section between two stations is divided differently depending on the signalling system used:

$$S = \begin{cases} \sum_{j=1}^{M} l_j, & \text{if the signalling system is ETCS Level2} \\ \zeta \cdot \Delta s, & \text{if the signalling system is MBS, with } \Delta s \leq \frac{v_{\min}^2}{2a_{\text{bra}}} \end{cases} \tag{1}$$

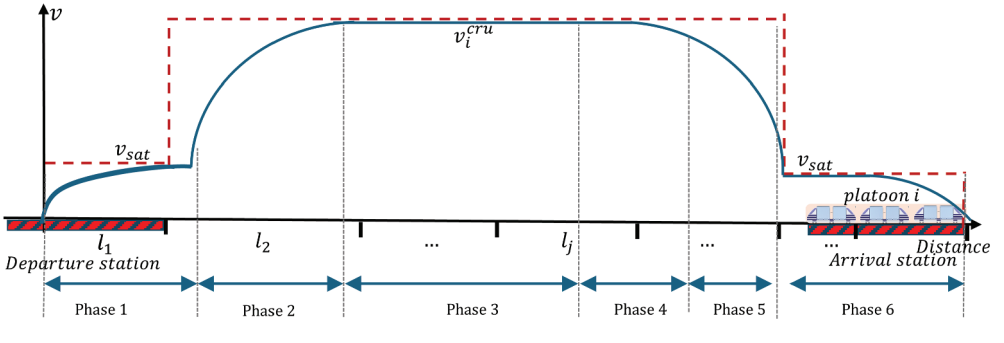

Figure 5. Pods operation phase between two stations.

In ETCS Level 2, the line is divided into fixed length blocks l_j, each protected by a trackside radio block centre. In contrast, MBS (Moving Block System) enables dynamic adjustment of train separation by continuously calculating the safe braking distance in real time. As a result, ζ uniform segments of length Δs. The discretization step in MBS is based on the minimum required braking distance, ensuring that the segment length Δs does not exceed $\frac{v_{\min}^2}{2a_{\text{bra}}}$, where $v_{\min}$ is the minimum operating speed and a_{bra} is the maximum allowed deceleration rate.

To establish a unified model that accommodates both scenarios, a universal index j is introduced to denote each discretized segment, with a length of Δs_j defined as a physical block length for ETCS Level 2 or a constant step size for MBS. At each discrete point j, the platoon i updates its velocity and position based on the following rules:

$$v_{i,j} = v_{i,j-1} + \frac{a_{i,j}\left(\Delta s_j + \Delta s_{\text{req}}^{(i,j-1)}\right)}{max\left\{v_{i,j-1}, \varepsilon\right\}} \tag{2}$$

$$L_j^{\text{total}} = L_{j-1}^{\text{total}} + \Delta s_j \tag{3}$$

where ε is a small positive constant used to prevent division by zero, L_j^{total} is the cumulative distance from the departure station to the start of block j.

The remaining distance $\Delta s_{\text{req}}^{(i,j)}$ required to complete the acceleration or braking of the platoon i in the block j is calculated as follows:

$$\Delta s_{\text{req}}^{(i,j)} = \begin{cases} \max\left(0, \frac{\left(v_{i,j}^{\text{out}}\right)^2 - \left(v_{i,j}\right)^2}{2a_{i,j}} - l_j\right), & \text{if the system is ETCS Level2} \\ 0, & \text{if the system is MBS} \end{cases} \tag{4}$$

The platoons follow a nominal trajectory comprising acceleration, cruise, and braking stages, as illustrated in Figure 5. At each discretized position j, the instantaneous acceleration $a_{i,j}$ for the platoon i is adaptively determined based on the pervious speed $v_{i,j-1}$, the position L_j^{total} and the target cruising speed v_i^{cru}. Instantaneous acceleration $a_{i,j}$ is determined by current speed $v_{i,j-1}$ and position s_{j-1}, following a standard acceleration – cruise – braking profile across the sections between two stations, as defined below:

$$a_{i,j} = \begin{cases} a_{\text{tra}}, & \text{if } L_{j-1}^{total} = 0 \wedge v_{i,j-1} \leq v_{sta} + \delta_v \ \text{(a)} \\ & \vee\, v_{i,j-1} \leq v_i^{cru} \wedge L_{j-1}^{total} \geq L_{sta,de} \ \text{(b)} \\ 0, & \text{if} \left|v_{i,j-1} - v_{sta}\right| \leq \delta_v \wedge L_{j-1}^{total} \leq L_{sta,de} \ \text{(c)} \\ & \vee \left|v_{i,j-1} \leq v_i^{cru}\right| \leq \delta_v \wedge v_{i,j-1} \geq v_{\min} \ \text{(d)} \\ & \vee \left|v_{i,j-1} - v_{sta}\right| \leq \delta_v \wedge L_{j-1}^{total} \geq S - \frac{v_{i,j-1}^2 - v_{sta}^2}{2a_{bra}} \ \text{(e)} \\ a_{bra}, & \text{if } v_{i,j-1} \geq v_{\min} \wedge S - L_{j-1}^{total} \leq \frac{v_{i,j-1}^2 - v_{sta}^2}{2|a_{bra}|} \ \text{(f)} \\ 0, & \text{otherwise (g)} \end{cases} \tag{5}$$

Equation (5) defines a piecewise acceleration rule that governs phase transitions in the speed profile of each platoon. Condition (a) applies when the train leaves the station and its speed is below the station limit v_{sta}, in which case the pods need to accelerate to pass the station section. Condition (b) keeps the acceleration active after leaving the station if the current speed remains below the cruising speed v_i^{cru}. Conditions (c), (d), and (e)

describe scenarios in which the rail pods enter a constant-speed phase. Specifically, (c) corresponds to the transition from acceleration to cruising; (d) captures steady cruising when the speed stabilizes around the desired cruising speed v_i^{cru}; and (e) represents the preparation phase for braking as the train approaches the destination station. Condition (f) triggers active braking a_{bra} when the remaining distance is insufficient to safely decelerate to v_{sta}. Finally, (g) applies to all other cases.

The running time on each discrete segment, $\Delta \mathrm{T}_{\mathrm{i,j}}$, for the pod platoon i passing through the segment j is calculated as follows:

$$\Delta T_{i,j} = \frac{\Delta \mathrm{s}_j + \Delta \mathrm{s}_{\mathrm{req}}^{(j-1)}}{v_{i,j}} \tag{6}$$

3.4. Infrastructure occupation calculation model

The blocking-time theory quantifies infrastructure occupation by defining the total duration a train renders a block section unusable [29,42,43] evaluating. However, this framework assumes fixed train lengths and an operation time, which limits its applicability to dynamic formation and reconfigurable pod platoons. To overcome this limitation, we extend the classical blocking-time theory to account for platoon composition with variable lengths and internal spacing. Figure 6 illustrates the spatio-temporal blocking profiles for a pod platoon operating under two typical scenarios: (a) cruising and (b) station approach and departure. In each subfigure, the top part presents the speed profile across segmented infrastructure blocks, while the bottom part visualizes the corresponding block occupation timeline.

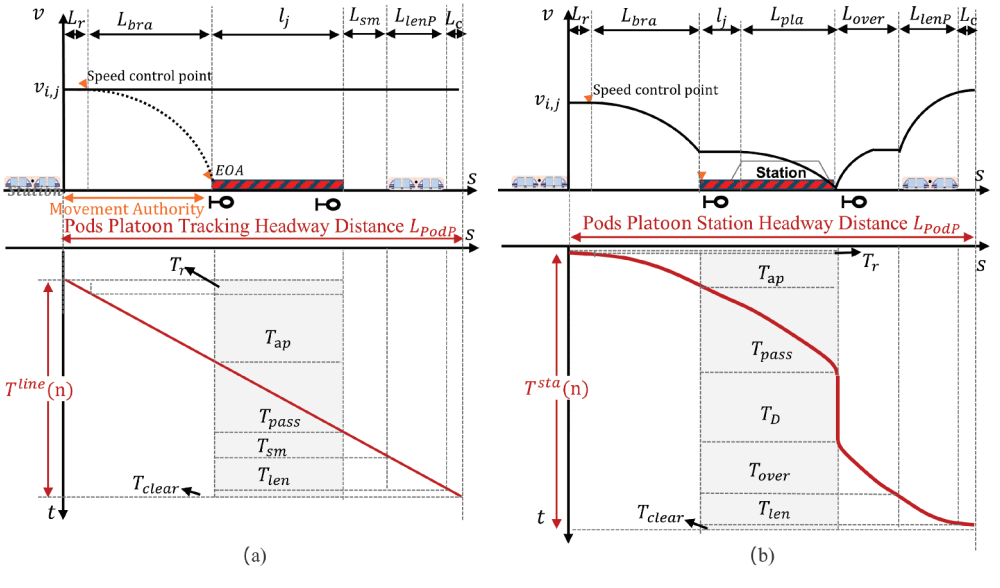

Figure 6. Block occupancy diagram for pod platoon traffic with different sizes: (a) the track blocking time for a pod platoon, (b) the station blocking time for a pod platoon.

For cruising segments (Figure 6a), the block occupation time for a pod platoon is governed by:

$$T^{\text{line}}(n) = T_{\text{r}} + \frac{v_i^{\text{cru}}}{a_{\text{bra}}} + \frac{l_{\text{j}} + nL_{\text{lenP}} + (n-1)S_{\text{intra}} + L_{\text{sm}}}{v_i^{\text{cru}}} + T_{\text{clear}} \tag{7}$$

Here, nL_{lenP} represents the total physical length of pod vehicles within a platoon, while $(n-1)S_{\text{intra}}$ denotes the safety separations between adjacent pods in the platoon. The term L_{sm} denotes the fixed safety margin distance, defined based on the underlying theoretical framework to account for position uncertainty and communication delays within the signalling system (50 to 200 m) [15]. Other components, such as reaction time T_{r}, approaching time, and release delay, are governed by the real-time coordination system and are considered independent of the platoon size. Accordingly, the model captures how larger platoon formations lead to extended occupation, critical for capacity estimation and control design.

For station segments (Figure 6b), additional components must be considered, including dwell time and constrained acceleration profiles. The blocking time of a pod platoon is:

$$T^{sta}(n) = T_r + \frac{v_i^{cru}}{a_{bra}} + \frac{L_{pla} - \frac{(v_i^{cru})^2}{2a_{bra}}}{v_i^{cru}} + T_D + T_{\text{over}} + T_{len} + T_{clear} \tag{8}$$

When generalized to an n-pod platoon, the time required to fully clear the station throat increases proportionally to the platoon length. To ensure safe operations and avoid conflicts, the station overlap length must be correspondingly extended. Given the allowable station speed and the overlap length, the rear-end passing time of the pod platoon through the station and overlap sections is computed as follows:

$$T_{\text{over}} + T_{\text{len}} = \begin{cases} \sqrt{\frac{2(nL_{\text{len P}} + (n-1)S_{\text{intra}} + L_{\text{over}})}{a_{\text{tra}}}}, & v_i^{\text{cru}} \geq V_{\text{crit}}, \\ \frac{2a_{\text{tra}}(nL_{\text{len P}} + (n-1)S_{\text{intra}} + L_{\text{over}}) + (v_i^{\text{cru}})^2}{2a_{\text{tra}} v_i^{\text{cru}}}, & v_i^{\text{cru}} < V_{\text{crit}}. \end{cases} \tag{9}$$

where V_{crit} denotes the critical velocity defined by:

$$V_{\text{crit}} = \sqrt{2a_{\text{tra}}(nL_{\text{lenP}} + (n-1)S_{\text{intra}} + L_{\text{over}})}.$$

Convert to Display Compared to cruising segments, station areas exhibit higher sensitivity to platoon length due to the complexity of station throat sections and overlap track areas. Capturing this effect through an extended formulation is crucial to accurately evaluate infrastructure capacity under operational and signalling constraints.

3.5. Cruising speed optimization for infrastructure occupation minimization

Figure 7 illustrates the operational concept with different size pod platoons. Each pod cruises at an optimized speed v_i^{cru}. Blue curves indicate the braking speed curve at the recommended cruising speeds, while red dashed lines denote protection speed limits computed from the signalling system. Safety margins (red blocks) and dynamically coordinated headways (green segments) ensure safe separation between platoons. By

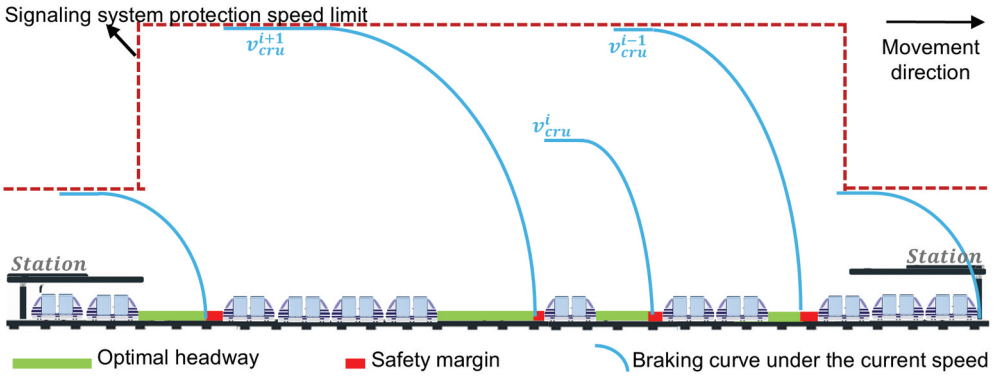

Figure 7. Operational concept of hybrid-structured rail pod platoons.

adjusting cruising speeds in coordination with the platoon structure, headways can be balanced to reduce overall infrastructure occupation. To quantitatively evaluate capacity under such dynamic conditions, this section introduces an optimization-based model that minimizes the infrastructure occupation while satisfying safety and signalling constraints.

3.5.1. Model formulation

The capacity consumed by a given pods' service schedule is measured by the total time the infrastructure is occupied. Thus, a capacity-effective schedule aims to minimize the infrastructure occupation. Assuming a fixed start time for the rail pods' service, this translates into reducing the time when the last platoon in a schedule cycle clears the considered infrastructure. Given a section composed of M blocks, the objective is to calculate the capacity consumption of N pod platoons, where each platoon consists of n pods. The objective function is defined as:

$$\min T_{\text{pass}} = t_{N,M} - t_{1,0} \tag{10}$$

where the total passing time T_{pass} is calculated through an iterative process on platoon movements and block transitions. The term $t_{1,0}$ represents the initial timestamp when the first platoon ($i = 1$) is ready to enter the first block (in state $j = 0$).

For each block j, the earliest time at which the platoon i can enter is determined by the time headway $h_{\text{opt}}(i-1, j)$ from the preceding platoon:

$$t_{i,j} = t_{i-1,j} + h_{opt}^{(i-1,j)} \quad \forall i \in I,\ j \in J \tag{11}$$

The total passing time of pod platoon i across M consecutive blocks is calculated based on its entry time into the first block $t_{i,1}$, as follows:

$$t_{i,M} = t_{i,1} + \sum_{j=1}^{M} T_{i,j}^{\text{pass}} \qquad \forall i \in \mathcal{I} \tag{12}$$

The recommended time headway $h_{\text{opt}}^{(i-1,j)}$ is imposed to maintain safe separation by ensuring that it exceeds the block occupation time of the preceding platoon. The term $T_{i-1,j}^{\text{block}}$ represents the blocking time of platoon $i-1$ in the block j, derived in Section 3.3.

It depends on the recommended speed profile and the composition of the platoon. Let α_j be a binary parameter that distinguishes block types: $\alpha_j = 1$ for regular inter-station blocks and $\alpha_j = 0$ for station blocks. The block occupation time is then calculated as

$$T_{i,j}^{\text{block}} = \alpha_j T_{i,j}^{T^{\text{line}}}(n) + \left(1 - \alpha_j\right) T_{i,j}^{T^{\text{sta}}}(n) \qquad \forall i \in \mathcal{I}, j \in \mathcal{J} \tag{13}$$

where $T_{i,j}^{\text{line}}(n)$ and $T_{i,j}^{\text{sta}}(n)$ are given by Equations (7) and (8), respectively.

The entire operation process is subject to the following constraints for all platoons $i \in \mathcal{I}$ and block segments $j \in \mathcal{J}$:

$$v_{i,j+1}^{\text{in}} = v_{i,j}^{\text{out}}, \qquad \forall i \in \mathcal{I}, j \in \{1, \ldots, J-1\} \tag{14}$$

$$t_{1,1} = 0 \tag{15}$$

$$V_{\min} \leq v_{i,j}^{\text{in}}, v_{i,j}^{\text{out}} \leq V_{\max}, \qquad \forall (i,j) \in \mathcal{I} \times \mathcal{J} \tag{16}$$

$$v_i^{\text{cru}} \geq v_{\text{sta}}, \qquad \forall i \in \mathcal{I} \tag{17}$$

$$h_{\text{opt}}^{(i-1,j)} \geq T_{i,j}^{\text{block}}, \qquad \forall i \in \mathcal{I} \backslash \{1\}, j \in \mathcal{J} \tag{18}$$

$$t_{i,j+1} = t_{i,j} + T_{i,j}^{\text{pass}}, \qquad \forall i \in \mathcal{I}, j \in \{1, \ldots, J-1\} \tag{19}$$

$$t_{i,j} \geq t_{i-1,j} + h_{\text{opt}}^{(i-1,j)}, \qquad \forall i \in \mathcal{I} \backslash \{1\}, j \in \mathcal{J} \tag{20}$$

Specifically, Equation (14) ensures velocity continuity across blocks. Equation (15) sets the initial departure time of the lead platoon to zero, serving as a temporal reference. Speed limits are enforced through Equation (16), while Equation (17) ensures that the cruising speed is above the minimum station speed. Equation (18) maintains safe headway separation based on the dynamic block time of the preceding platoons. To ensure trajectory continuity and temporal feasibility across blocks, Equation (19) recursively defines the entry time to each block based on the running time of the preceding block. Finally, Equation (20) imposes a minimum headway time between successive platoons within the same block, preventing trajectory conflicts.

3.5.2. Solution

As illustrated in Figure 5, each platoon follows a structured speed profile comprising the traction, cruising, and braking phases. To mathematically formulate this profile, a state-dependent control rule, as detailed in Equation (5), determines the acceleration $a_{i,j}$ for each block. This acceleration is then used to calculate the block running time $T_{i,j}^{\text{pass}}$ and the exit speed $v_{i,j}^{\text{out}}$ using the movement update rules according to Equations (2), (3) and (6). Specifically, the appropriate traction, cruising, or braking phase is selected by determining the corresponding acceleration value, based on an evaluation of the train's current state against operational thresholds and its designated cruising speed. This determined acceleration is then substituted into the kinematic update Equations (2) and (3) to calculate the block pass time and the exit speed. Furthermore, the total passing

time T_{pass} can be expanded under the ETCS-2 operation system into closed-form expressions based on the same control rule, as detailed in Appendix A. These expressions enable direct evaluation of T_{pass} and corresponding speed within the solution procedure.

In the proposed model, cruise speed v_i^{cru} and time headway $h_{\text{opt}}^{(i,j)}$ are introduced as decision variables. The headway $h_{\text{opt}}^{(i,j)}$ determines the entry time of platoon i in block j, subject to a block occupation time of the preceding platoon. This formulation supports adaptive adjustment of the temporal spacing between platoons while remaining within the safe operational limits. The optimization problem involves nonlinear coupling among cruising speed, running time, platoon entry timing, and safety headway, which creates a non-convex feasible region and makes it difficult to directly apply conventional solvers. However, since the number of constraints remains moderate compared to the dimensionality of the decision space, a hybrid Interior Point–Augmented Lagrangian method is adopted to solve the problem.

The augmented Lagrangian function is defined as:

$$\mathcal{L}(\mathbf{x},\mu,\rho) = \underbrace{t_{N,M} - t_{1,1}}_{\text{Eq.}(10)} - \mu \sum_{k\in\mathcal{K}} \ln\, c_k(\mathbf{x}) + \frac{\rho}{2}(\Psi_v + \Psi_t) \tag{21}$$

where $c_k(\boldsymbol{x}) \geq 0$ represents an individual inequality constraint of the model. The summation is performed on the index k of the set $\mathcal{K}$, which is the comprehensive index set containing all inequality constraints, including all speed limits and headway bounds. To enforce equality constraints, quadratic penalties are introduced:

$$\Psi_v = \sum_{i=1}^{N}\sum_{j=1}^{M-1}\left(v_{i,j+1}^{\text{in}} - v_{i,j}^{\text{out}}\right)^2 \tag{22}$$

$$\Psi_t = \sum_{i=1}^{N}\sum_{j=2}^{M}\left(t_{i,j} - \left(t_{i,j-1} + T_{i,j-1}^{\text{pass}}\right)\right)^2 \tag{23}$$

A quasi-Newton method is employed to iteratively solve the augmented Lagrangian function. The iteration terminates once the following conditions are met:

$$\begin{cases} \mu^{(t)}\left|\sum_{k\in\mathcal{K}} \ln c_k(\boldsymbol{x}^{(t)})\right| < 10^{-6}, \\ \|\nabla\mathcal{L}(\boldsymbol{x}^{(t)})\|_2 < 10^{-4}, \\ \max_{(i,j)}\left|v_{i,j+1}^{\text{in}} - v_{i,j}^{\text{out}}\right| < 10^{-5} \end{cases} \tag{24}$$

Table 3 outlines the algorithmic procedure used to solve the model. The algorithm employs an interior-point method embedded within a multi-start strategy to avoid local optima. Each initial guess, denoted as $(x^{(0)})$, comprises a set of initial cruising speeds and time headways.

Table 3. Interior-point augmented Lagrangian algorithm for pods capacity optimization.

Input:

A set of initial guesses values for Decision Variables, $S = \{\boldsymbol{x}_1^{(0)}, \boldsymbol{x}_2^{(0)}, \ldots\}$, where each $\boldsymbol{x}^{(0)}$ contains initial *cruising speeds* and *time headways*.

Initial barrier parameter $\mu^{(0)} > 0$, penalty parameter $\rho^{(0)} > 0$.

Tolerances $\varepsilon_1, \varepsilon_2, \varepsilon_3 > 0$ for the *Converge Check* module.

Output:

Solution $\boldsymbol{x}_{\text{best}}$, representing the final optimal *cruising speeds* and *time headways*.

Initialize Multi-start Environment:
    Initialize best-found objective value: $f_{\text{best}} \leftarrow \infty$.
    Initialize best-found solution (speeds, headways): $\boldsymbol{x}_{\text{best}} \leftarrow$ null.
For each initial guess $\boldsymbol{x}^{(0)}$ in the set S: *(Outer loop for multi-start strategy)*
    — Begin single optimization run from a given starting point —
    Initialize variables for this run: $t \leftarrow 0$; $\boldsymbol{x} \leftarrow \boldsymbol{x}^{(0)}$ (set current *speeds* and *headways*); $\boldsymbol{H} \leftarrow \boldsymbol{I}$.
    Repeat until convergence criteria are met: *(Main solver loop from Figure 4)*
        Construct augmented Lagrangian $\mathcal{L}(\boldsymbol{x}, \mu, \rho)$ based on the current *speeds* and *headways*.
        (This step performs the 'Candidate Solution Evaluation' using the blue modules in Figure 4)
        Compute search direction $\boldsymbol{d}$ and step size η.
    Update Decision Variables: $\boldsymbol{x} \leftarrow \boldsymbol{x} + \eta\boldsymbol{d}$ (generate new candidate *speeds* and *headways*).
    (Steps 9–10 correspond to the 'Generate new candidate' feedback path in Figure 4)
    Update penalty ρ, barrier μ, and Hessian $\boldsymbol{H}$ parameters.
    $t \leftarrow t + 1$.
    — End single optimization run —
Let $\boldsymbol{x}^*$ be the converged solution for this run.
If objective value $f(\boldsymbol{x}^*) < f_{\text{best}}$:
$\boldsymbol{x}_{\text{best}} \leftarrow \boldsymbol{x}^*$ (store the better set of *speeds* and *headways*).
$f_{\text{best}} \leftarrow f(\boldsymbol{x}^*)$.
Final Verification Step:
Verify physical feasibility of $\boldsymbol{x}_{\text{best}}$ (e.g., check speed $|v_{i,j}| \leq v_{\max}$ resulting from the optimal *speeds*).
If not feasible, discard solution or flag for review.
Return $\boldsymbol{x}_{\text{best}}$.

4. Case study and results

While the model framework supports multiple signalling paradigms, including the ETCS level 2 signalling system and moving block systems, we restrict algorithmic implementation and simulation to the ETCS level 2 signalling system. This choice reflects two practical considerations. First, the ETCS level 2 signalling system remains the most widely deployed standard in European rail freight corridors and thus serves as a realistic testbed. Second, continuous updates inherent in the moving block system introduce additional real-time constraints and communication dependencies that fall outside the scope of this study but are earmarked for future work. Related parameters are reported in Table 4.

The optimization framework was implemented in MATLAB on a standard PC (Intel Core i7, 16 GB RAM). The Hybrid Interior-Point algorithm was initialized with a penalty parameter $\rho^{(0)} = 10$, a barrier parameter $\mu^{(0)} = 0.1$, and convergence tolerances $\varepsilon_1 = 10^{-6}$ and $\varepsilon_2 = 10^{-4}$ as defined in Equation (24). For the case study scenarios, the algorithm converged within fewer than 10 iterations (e.g., 8 iterations in the baseline scenario). The average computation time for a single schedule optimization was approximately 3 s.

Table 4. Simulation parameters for case study.

Symbol	Value (Unit)	Symbol	Value (Unit)	Symbol	Value (Unit)
Pod Characteristics		**Dynamic Constraints**		**Operational Limits**	
Block No.	6 (-)	a_{bra}	1.0 (m/s ^{2})	v_{sta}	20 (m/s)
L_{tlen}	100 (m)	a_{tra}	0.8 (m/s ^{2})	v_{max}	60 (m/s)
S_{intra}	30 (m)			v_{min}	20 (m/s)
Geometric Layout		**Control Parameters**		**Time Constants**	
l_j	[1000, 1500 × 4, 1000] (m)	T_r	4 (s)	T_{stop}	30 (s)
L_{pla}	100 (m)	T_{clear}	3 (s)	t_{couple}	90 (s)
L_{over}	50 (m)				
L_{sm}	200 (m)				

4.1. Analysis of the relation capacity-cruising speed for uniform pod platoons

First, consider a uniform platoon configuration in which each platoon consists of the same number of pods, resulting in equal platoon lengths. By excluding the complexity of different platoon lengths and varying coordinated speed adjustments, this part of the analysis serves as a baseline scenario to examine the fundamental relationship between cruising speed, platoon size, and infrastructure occupation, as captured in Equation (7). In a configuration with uniform block section length, the minimum headway time equals the block occupation time, leading to a line headway defined as $H^{\text{linep}} = T_{i,j}^{\text{block}}$. The corresponding line capacity is derived from the UIC standard as follows:

$$C_{\text{line}} = \frac{3600}{H^{\text{linep}}} \tag{25}$$

Based on this formulation, we systematically vary the platoon length to analyse its influence on headway time and capacity. The relationship between platoon speed, optimized headway time, and line capacity under different platoon lengths is illustrated in Figure 8.

The results reveal that increasing the platoon size directly enlarges the inter station cruising segments headway time (also called tracking headway time), especially in low-speed scenarios (e.g., 20–40 m/s). The tracking headway time exhibits a non-linear relationship with speed. At low speeds, an increase in speed can significantly reduce

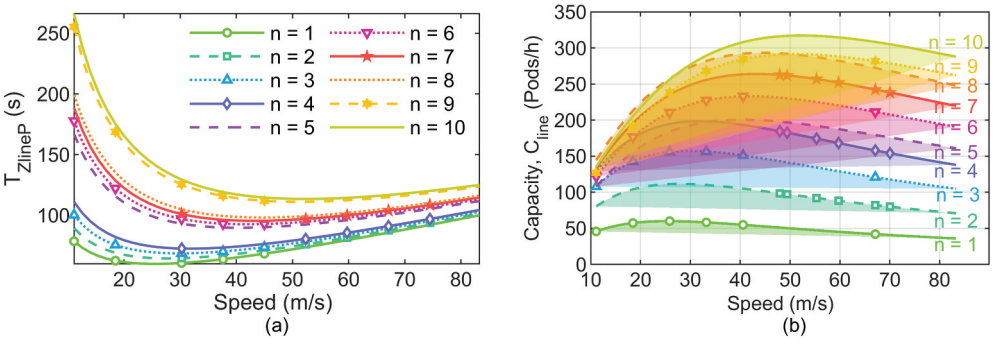

Figure 8. Impact of platoon length on speed, headway, and capacity of inter station cruising segments: (a) minimal time headway varies with speed for platoon with *n* pods, (b) capacity varies with speed for platoon with *n* pods.

the headway time, as the time component associated with the braking distance is insignificant, while the time required to traverse the length of the block section is the dominant factor. However, at higher speeds, the effect of the rapidly increasing braking distance outweighs this, causing the total headway to increase. Although increasing the size of the platoon generally enhances the capacity of the inter station cruising segments, an excessively long tracking headway time may diminish this benefit; as the headway time increases non-linearly with platoon size, capacity improvement slows down and may even reverse. Therefore, there exists a critical speed that optimizes the trade-off between the tracking headway time and capacity, indicating that a speed threshold existed for maximum efficiency under a given platoon configuration.

Figure 8 shows that headway requirements vary substantially with platoon length. At 40 m/s, the minimum headway increases from about 60 s for $n = 1$ to nearly 120 s for $n = 10$. This difference has two implications. First, if a fixed 60 s headway is used based on single-pod behaviour, operating a long platoon would violate the necessary blocking time, resulting in a operational safety risk. Second, if a uniform 120 s headway is applied instead, single-pod operations would lose nearly 50% of potential capacity. These observations show that capacity assessment must account for platoon structures.

Further analysis is conducted on the relationship between speed, headway time, and capacity within the station section under uniform platoon flow conditions. Figure 9 illustrates the impact of the additional train separation constraints imposed by the safety-critical braking phase for a station stop, which is formulated in Equation (8).

The results indicate that the station capacity is not directly proportional to the speed or size of the platoons. As expected, the station capacity results to be lower than the section capacity, due to the limited approaching speeds usually imposed in the station areas. Consequently, when rail pods transition from station-constrained segments to open-line sections, the resulting capacity redundancy provides greater flexibility to adjust platoon formations through speed modulation. When a train forms platoons of different configurations, there will be varying supply rates within the time window for pod transportation.

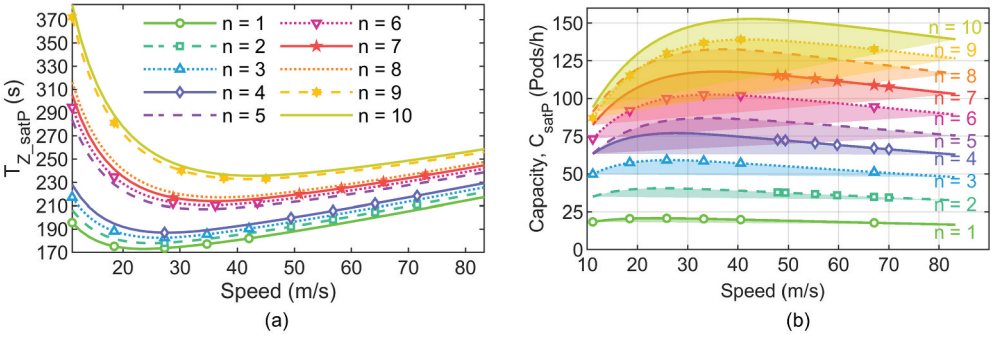

Figure 9. Impact of platoon length on speed, headway, and capacity of station segments: (a) minimal time headway varies with speed for platoon with n pods, (b) capacity varies with speed for platoon with n pods.

4.2. Capacity analysis of different pod platoon structures with optimized cruising speeds

To further evaluate the impact of different platoon configurations on infrastructure capacity, we consider all possible platoon arrangements composed of six pods under a fixed infrastructure setup. Specifically, test cases were generated by partitioning a set of six pods into different platoon configurations (e.g., one platoon of six, two platoons of three, or three platoons of two). This analysis is based on the optimization model of Equation (10), which determines the optimal cruising speeds and headways for each configuration. By listing all integer partitions of six pods, a total of 32 distinct platoon structures are generated, ranging from a single long platoon to multiple shorter, evenly distributed platoons. These configurations are used as input to the optimization model. Figure 10 shows the infrastructure occupation time corresponding to each configuration. The X-axis represents the total track occupation time, while the Y-axis indexes the specific platoon structures.

The comparison reveals that the platoon structure has a significant influence on infrastructure consumption. The most efficient configuration, identified through the comparative analysis of all feasible platoon structures in Figure 10, can improve system efficiency by up to 39.2%. These findings highlight the importance of structural design in platoon scheduling and provide a quantitative basis for future optimization in dynamic platoon management strategies. The results suggest that in the absence of platform length constraints, forming larger platoons can significantly enhance infrastructure utilization. Even when accounting for the additional occupation time required for coupling and

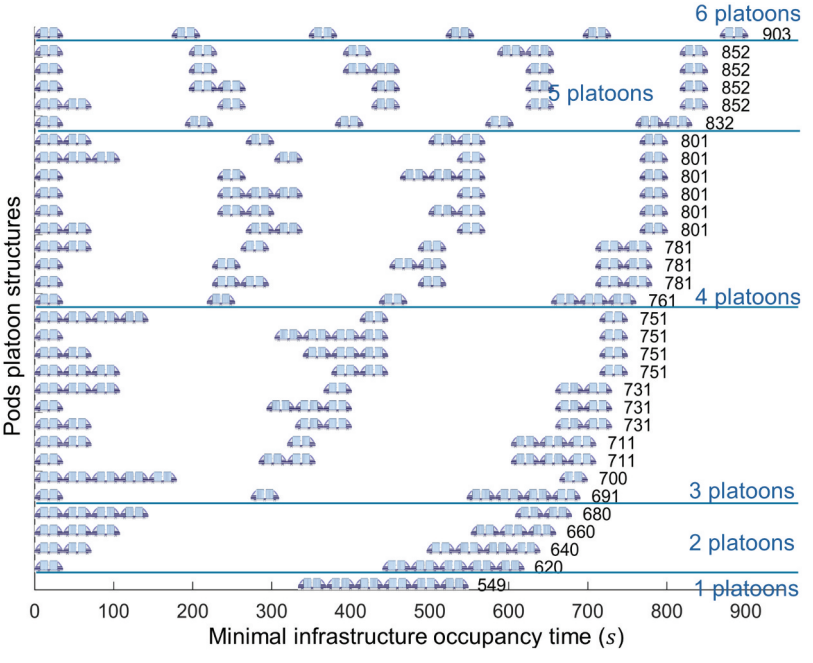

Figure 10. Minimum infrastructure occupation time for different size platoons.

decoupling operations at stations, the capacity gains associated with longer platoons remain substantial.

Even when partitioned into the same set of platoon sizes, the operational sequence of these platoons can lead to significant differences in infrastructure occupation. For instance, the 2–3–1 structure and the 1–1–4 structure both consist of three platoons, where numbers indicate the number of pods included in each platoon, but their temporal occupation across the blocking sections differs due to the order and size distribution of the platoons.

To investigate capacity-related effects, Figure 11 compares the block time occupation and optimized coordinated cruise speed for 2–3–1 and 1–1–4 Joint Undertaking platoon configurations. The horizontal axis denotes the cumulative length of the blocks, while the rectangular blocks represent the minimum safe separation time required by each block. The upper part of Figure 11 shows the safety separation and the speed profile of the block, and the lower part shows its coordinated speed configuration. Curved lines represent the coordinated speed profiles computed for each platoon. Each group of lines corresponds to one platoon, and the number of lines in each group reflects the number of pods within that platoon. The results indicate that optimized cruise speed configurations can minimize block occupation time in different platoon structures. The departure block often becomes the bottleneck in the overall capacity consumption. This is visually evident in Figure 11, where the occupation time of the first block (B1) for each platoon is markedly longer than that of the subsequent cruising blocks (e.g. T1-B1 at 210.0 s vs. T1-B2 at 126.9

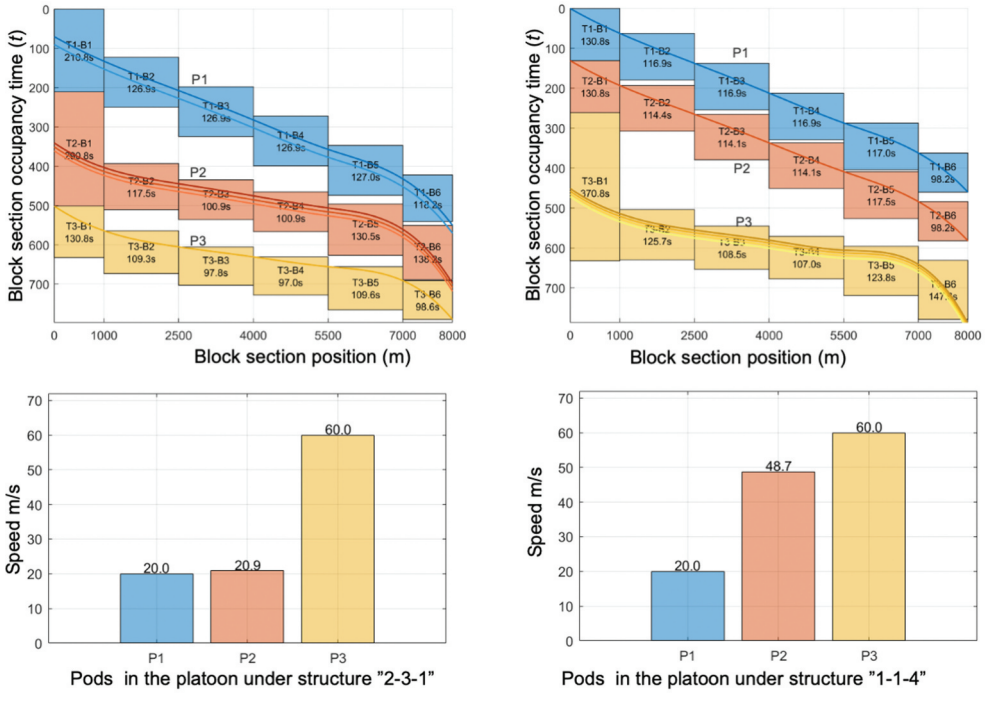

Figure 11. Block section occupancy and optimized cruise speeds under platoon structures "2–3–1" and "1–1–4".

s in the 2–3–1 case). This extended duration arises because an additional dwell time is incorporated in the departure block for pod platoon formation, which is proportional to the platoon size. This visualization highlights how structural layout and coordinated speed planning jointly impact infrastructure usage, reinforcing the need for formation and speed co-optimization in platoon scheduling.

Interestingly, the results from Figure 11 offer a counter intuitive insight: operating at maximum speed is not always necessary to achieve optimal capacity. Instead, the optimal strategy is 'slow-front, fast-rear' coordination, where leading platoons are assigned relatively lower speeds while following platoons travel faster. This arrangement reduces inter-platoon gaps by allowing faster rear platoons to catch up safely, thereby improving infrastructure utilization. The optimized speeds are not linearly proportional to platoon size, indicating that capacity depends on the coordinated optimization of structural layout and speed planning rather than on uniformly increasing speed.

The emergence of this strategy is driven by the optimization objective. Theoretically, the total infrastructure occupation time can be decomposed into two components: the cumulative headways of preceding platoons (indices 1 to $N-1$) and the running time of the final platoon (see Appendix B for the formal derivation). This reveals distinct optimization objectives. For preceding platoons, minimizing headways is critical; since the headway function is convex (see Figure 8 and 9), the optimizer targets a moderate capacity-optimal speed. In contrast, the final platoon ($i = N$) does not generate additional headway terms, since no platoon follows it, and therefore contributes only its own running time to the objective function; consequently, the optimizer selects the maximum admissible speed to minimize the total duration.

4.3. Sensitivity analysis of key parameters

To quantify the interaction effects of vehicle dynamics, infrastructure characteristics, and coupling time on system capacity, a joint sensitivity analysis was performed. The analysis evaluates how the minimum infrastructure occupation time and the resulting optimal platoon structures vary under the combined influence of three key variables, namely the block section length, the acceleration and the braking rates. Figure 12a illustrates the effect of dynamic performance, represented by a scaling factor γ applied to the acceleration rate (a_{tra}) and braking (a_{bra}) rates, which are varied from 0.5 to 1.5. Figure 12b reflects the influence of block section length by scaling block section lengths to represent physical lengths from 500 m to 1500 m. Across all scenarios, coupling time is varied from 30 s to 180 s.

As shown in Figure 12a, increasing the dynamic factor γ improves traction and braking performance, leading to a monotonic reduction in total occupation time. However, the shift between optimal structures is driven primarily by the coupling time. When coupling times are short, the model selects the 1×6 configuration, in which all six pod units operate as a single coupled platoon, thereby requiring only one block-occupation sequence. As coupling time increases, a threshold is reached where the formation delay exceeds these headway savings. Consequently, the solution switches to the 6×1 structure, where pods operate independently to bypass the coupling delay.

Figure 12b demonstrates that the infrastructure occupation and the selection of platoon structure are jointly governed by the interaction between block section length

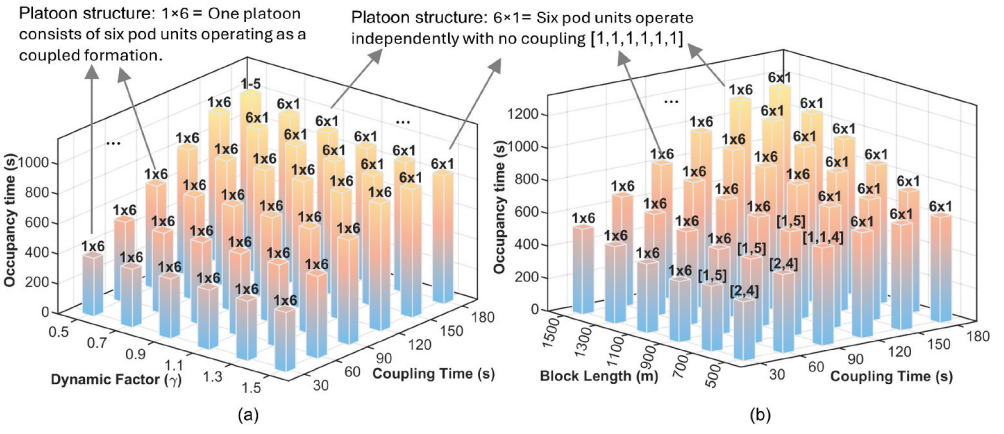

Figure 12. Sensitivity analysis of key parameters on infrastructure occupation time and platoon structures: (a) impact of dynamic factor and coupling time, (b) impact of block length and coupling time.

and coupling time. For short block sections such as 500 m, the baseline blocking time is already low, so the capacity gain from platooning is limited. For long block sections such as 1500 m, forming a single coupled platoon substantially reduces the number of block occupations. This larger capacity benefit allows the system to tolerate much longer coupling durations, and the [1,1,1,1,1,1] structure remains optimal for coupling times up to 150 s or beyond.

These findings indicate that the feasibility of platoon formation is jointly constrained by vehicle dynamics, infrastructure geometry, and coupling efficiency. Specifically, corridors with short block sections necessitate fast coupling mechanisms to be viable, whereas lines with longer blocks offer greater operational flexibility. This analysis provides a quantitative reference for defining feasible coupling windows and scheduling constraints tailored to specific infrastructure characteristics.

4.4. Benchmark comparison under constrained conditions

The coordinated speed optimization was benchmarked against a minimum travel time approach, where each pod runs independently at maximum power and permissible speed to minimize its own occupation time. The benchmark was conducted under constrained operating conditions with reduced braking capability (0.4 m/s^2) and short block sections (800 m), conditions under which high cruising speeds increase the required safety headway and reduce capacity. This setup assesses whether the optimization can adapt speeds to improve infrastructure utilization.

The results in Table 5 indicate that the proposed method adjusts speeds according to the characteristics of each platoon structure. For the high-density configuration [1,1,1,1,1,1], the method reduced the total occupation time by 37% through differentiated cruising speeds that reduced the average headway. For different structures, the algorithm identified structure-specific improvements, including a 6.7% reduction for the front-heavy [5,1] configuration and a 25.1% reduction for the balanced [2,2,2] configuration.

Table 5. Benchmark results under constrained conditions ($a_{bra} = 0.4$ m/s ^{2}, $l_{block} = 800$ m).

Structure	Strategy	Cruising Speeds (m/s)	Avg. Headway	Total Time	Improve
[1,1,1,1,1,1]	Proposed	[20.3, 24.5, 29.8, 35.2, 41.0, 60.0]	124.5 s	812.6 s	37.0%
	Bench ($v = 40$)	[40, 40, 40, 40, 40, 40]	130.5 s	852.5 s	–
	Bench ($v = 60$)	[60, 60, 60, 60, 60, 60]	229.9 s	1289.4 s	–
[5,1]	Proposed	[38.5, 60.0]	256.6 s	802.5 s	6.7%
	Bench ($v = 40$)	[40, 40]	270.5 s	861.5 s	–
	Bench ($v = 60$)	[60, 60]	320.6 s	860.3 s	–
[2,2,2]	Proposed	[32.4, 40.1, 60.0]	155.2 s	787.2 s	25.1%
	Bench ($v = 40$)	[40, 40, 40]	165.5 s	846.3 s	–
	Bench ($v = 60$)	[60, 60, 60]	264.9 s	1050.8 s	–
[6]	Proposed	[60.0]	–	739.7 s	0.0%
	Bench ($v = 40$)	[40]	–	798.7 s	–
	Bench ($v = 60$)	[60]	–	739.7 s	–

For the fully coupled [6] structure, the optimization retained the maximum speed, confirming that no unnecessary adjustments were made. These results demonstrate that coordinated speed optimization offers substantial advantages over fixed-speed strategies when the system operates under capacity-constrained conditions.

Collectively, these results provide a quantitative basis for formulating dispatching strategies. To maximize throughput, priority should be given to coupled formations on long-block corridors, whereas independent dispatching is effective for short-block areas to avoid bottlenecks. In constrained scenarios involving reduced pod braking capabilities and short block section lengths, the proposed approach of coordinating platoon speeds outperforms the conventional minimum travel time driving policy in terms of capacity effectiveness. Finally, although rail pods are shorter and more agile than conventional trains, the proposed capacity evaluation framework is grounded in general blocking time theory. Therefore, it is generic and readily applicable to conventional passenger trains with variable formations (e.g., EMUs), by adjusting input parameters such as coupling duration and unit lengths.

5. Conclusions

The deployment of the pod system demands a higher degree of flexibility to enable customer-oriented rail services and seamless integration with existing infrastructure. To ensure operational feasibility, scheduling strategies must align with infrastructure constraints, particularly the safety rule imposed by signalling systems. Given the dynamic characteristics of pods, such as the variable platoon size, the conventional capacity assessment method based on fixed headways and uniform train types is no longer sufficient. To address this, we extend the UIC 406 blocking time theory to support pod platoons. A novel optimization model is proposed to minimize infrastructure occupation time. The model constructs a mapping between the platoon structures, the speed profile, and capacity consumption, enabling joint optimization of the speed allocation. The model incorporates operational safety rules and piecewise velocity profiles reflecting the traction – cruise – brake process. A hybrid Interior Point–Augmented Lagrangian method is employed to solve the resulting nonlinear optimization problem. The results related to a case study using the ETCS-2 signalling system settings show that infrastructure consumption is not linearly correlated with either platoon size or speed. The

proposed coordinated speed optimization according to platoon structures can increase capacity utilization by up to 39.2%. Optimal solutions typically exhibit a 'slow-front, fast-rear' velocity pattern. In particular, operating all trains at maximum speed is neither necessary nor optimal.

Furthermore, the analysis reveals that platoon coupling time critically influences capacity efficiency and optimal platoon structure selection. Once coupling time exceeds a certain threshold, the benefits of platoon-based optimization diminish and introduce feedback constraints on the pickup and delivery windows in pod deployment. This study provides a quantitative foundation for evaluating the interaction between pod system features and infrastructure constraints. Future model applications involving heterogeneous pod characteristics or control strategies will require a detailed representation of individual braking and acceleration profiles, diverse pod masses, and the influence of track gradients and resistance forces along the route.

Acknowledgements

We would like to express our gratitude to our project partners and sponsors. The authors would also like to thank the reviewers for their valuable comments and suggestions on this manuscript.

Disclosure statement

The authors declare that they have no known competing financial interests or personal relationships that could have appeared to influence the work reported in this paper. Funded by the European Union. Views and opinion expressed are however those of the author(s) only and do not necessarily reflect those of the European Union or the Europe's Rail Joint Undertaking. Neither the European Union nor the granting authority can be held responsible for them. The project Pods4Rail project is supported by the Europe's Rail Joint Undertaking and its members.

Funding

This project has received funding from the European Union's Horizon Europe research and innovation programme under Grant Agreement No 101121853.

References

[1] Europe's Rail Joint Undertaking. Pods4Rail – developing a new kind of mobility system. 2024 [cited 2025 Jul 28]; Available from: https://rail-research.europa.eu/latest-news/pods4rail-developing-a-new-kind-of-mobility-system/
[2] European Commission. Pods4Rail project — CORDIS. 2023 [cited 2025 Jul 28]; Available from: https://cordis.europa.eu/project/id/101121853
[3] Hassannayebi E, Sajedinejad A, Mardani S. Urban rail transit planning using a two-stage simulation-based optimization approach. Simul Modell Pract Theory. 2014;49:151–166. doi: 10.1016/j.simpat.2014.09.004
[4] Li X, Lo HK. Energy minimization in dynamic train scheduling and control for metro rail operations. Transp Res Part B. 2014;70:269–284. doi: 10.1016/j.trb.2014.09.009
[5] Özbakr L, Tapkan P, Kulluk S, et al. A modelling approach to the train timetabling problem using adaptive headways for dynamic passenger demand. Int J Rail Transp. 2022;10(5):606–630. doi: 10.1080/23248378.2021.1992802
[6] Pods4Rail Consortium. Pods4Rail project homepage. 2025 [cited 2025 Apr 23].

[7] Liao X, Han J, Martinez AP, et al. Unlocking the potentials of modularity in railways, a heuristic framework for pods scheduling. In: 2024 IEEE 27th International Conference on Intelligent Transportation Systems (ITSC), Edmonton, AB, Canada. IEEE; 2024. p. 2731–2736.
[8] Liao X, Han J, Saeednia M. Modular vehicle routing on railways: opportunities for intermodality. In: 2024 IEEE 27th International Conference on Intelligent Transportation Systems (ITSC), Edmonton, AB, Canada. IEEE; 2024. p. 572–577.
[9] UIC U. Code 406: Capacity. Paris: International Union of Railways; 2004.
[10] Flammini F, Marrone S, Nardone R, et al. Towards railway virtual coupling. In: 2018 IEEE International Conference on Electrical Systems for Aircraft, Railway, Ship Propulsion and Road Vehicles & International Transportation Electrification Conference (ESARS-ITEC), Nottingham, UK. IEEE; 2018. p. 1–6.
[11] Quaglietta E, Wang M, Goverde RM. A multi-state train-following model for the analysis of virtual coupling railway operations. J Rail Transp Plann Manag. 2020;15:100195. doi: 10.1016/j.jrtpm.2020.100195
[12] Wu L, Ye H, Dong W, et al. An optimal scheduling method for heavy haul trains with virtual coupling technology. Int J Rail Transp. 2025;13(4):682–707. doi: 10.1080/23248378.2024.2400173
[13] Nold M, Corman F. Dynamic train unit coupling and decoupling at cruising speed: systematic classification, operational potentials, and research agenda. J Rail Transp Plann Manag. 2021;18:100241. doi: 10.1016/j.jrtpm.2021.100241
[14] Di Meo C, Di Vaio M, Flammini F, et al. Ertms/Etcs virtual coupling: proof of concept and numerical analysis. IEEE Trans Intell Transp Syst. 2019;21(6):2545–2556. doi: 10.1109/TITS.2019.2920290
[15] Quaglietta E, Spartalis P, Wang M, et al. Modelling and analysis of virtual coupling with dynamic safety margin considering risk factors in railway operations. J Rail Transp Plann Manag. 2022;22:100313. doi: 10.1016/j.jrtpm.2022.100313
[16] Ning Z, Ou D, Xie C, et al. Optimal convoy composition for virtual coupling trains at junctions: a coalition formation game approach. Transp Res Part C. 2023;154:104277. doi: 10.1016/j.trc.2023.104277
[17] Chen Z, Li X. Designing corridor systems with modular autonomous vehicles enabling station-wise docking: discrete modeling method. Transp Res Part E. 2021;152:102388. doi: 10.1016/j.tre.2021.102388
[18] Lin J, Zhang F. Modular vehicle-based transit system for passenger and freight co-modal transportation. Transp Res Part C. 2024;160:104545. doi: 10.1016/j.trc.2024.104545
[19] Tian Q, Lin YH, Wang DZ. Joint scheduling and formation design for modular-vehicle transit service with time-dependent demand. Transp Res Part C. 2023;147:103986. doi: 10.1016/j.trc.2022.103986
[20] Jodeau J, Absi N, Chevrier R, et al. The rail-road dial-a-ride problem. Eur J Oper Res. 2024;318(2):486–499. doi: 10.1016/j.ejor.2024.05.036
[21] Zhang Z, Tafreshian A, Masoud N. Modular transit: using autonomy and modularity to improve performance in public transportation. Transp Res Part E. 2020;141:102033. doi: 10.1016/j.tre.2020.102033
[22] Zhou H, Li Y, Ma C, et al. Modular vehicle routing problem: applications in logistics. Transp Res Part E. 2025;197:104022. doi: 10.1016/j.tre.2025.104022
[23] Fu Z, Chow JY. Dial-a-ride problem with modular platooning and en-route transfers. Transp Res Part C. 2023;152:104191. doi: 10.1016/j.trc.2023.104191
[24] Zheng H, Li J, Lin J, et al. Exploiting modularity for co-modal passenger-freight transportation. Transp Res Part B: Methodological. 2025;196:103217. doi: 10.1016/j.trb.2025.103217
[25] Zheng S, Liu Y, Zhou Z, et al. Last mile passenger and freight synergistic and mobile distribution via modular autonomous vehicles. IEEE Trans Intell Transp Syst. 2025:1–15. doi: 10.1109/TITS.2025.3560313

[26] Hansen I, Pachl J. Railway timetabling and operations: analysis, modelling, optimisation, simulation, performance, evaluation. Eurail press; 2014.
[27] Landex A. Evaluation of railway networks with single track operation using the UIC 406 capacity method. Netw Spat Econ. 2009;9(1):7–23. Available from: https://api.semanticscholar.org/CorpusID:108512316
[28] Widyastuti H, Budhi W. Railway capacity analysis using Indonesian method and UIC code 405 method. In: IOP Conference Series: Materials Science and Engineering, Surabaya, Indonesia. IOP Publishing; 2020. Vol. 930. p. 012059.
[29] Bešinović N, Goverde RM, Quaglietta E. Microscopic models and network transformations for automated railway traffic planning. Comput Aided Civ Eng. 2017;32(2):89–106. doi: 10.1111/mice.12207
[30] Sameni MK, Landex A, Preston J. Developing the UIC 406 method for capacity analysis. Proceedings for 4th International Seminar on Railway Operations Research; 2011; Rome, Italy; 2011.
[31] Secretary T. H. E., Transportation O. F. Vision for high-speed rail in America. Environ. Rev. 2009.
[32] Gašpark J, Zitrický V. A new approach to estimating the occupation time of the railway infrastructure. Transport. 2010;25(4):387–393. doi: 10.3846/transport.2010.48
[33] Azadi Moghaddam Arani A, Jolai F, Nasiri MM. A multi-commodity network flow model for railway capacity optimization in case of line blockage. Int J Rail Transp. 2019;7(4):297–320. doi: 10.1080/23248378.2019.1571450
[34] Azadi Moghaddam Arani A, Jolai F, Nasiri MM. Reinforcement learning approach for train rescheduling on a single-track railway. Transp Res Part B: Methodological. 2016;86:250–267.
[35] Khadilkar H. A scalable reinforcement learning algorithm for scheduling railway lines. IEEE Trans Intell Transp Syst. 2018;20(2):727–736. doi: 10.1109/TITS.2018.2829165
[36] Ghasempour T, Nicholson GL, Kirkwood D, et al. Distributed approximate dynamic control for traffic management of busy railway networks. IEEE Trans Intell Transp Syst. 2020;21(9):3788–3798. doi: 10.1109/TITS.2019.2934083
[37] Ranjbar V, Olsson NO, Sipilä H. Impact of signalling system on capacity–comparing legacy ATC, ETCS level 2 and ETCS hybrid level 3 systems. J Rail Transp Plann Manag. 2022;23:100322. doi: 10.1016/j.jrtpm.2022.100322
[38] Luan X, Wang Y, De Schutter B, et al. Integration of real-time traffic management and train control for rail networks-part 1: optimization problems and solution approaches. Transp Res Part B: Methodological. 2018;115:41–71. doi: 10.1016/j.trb.2018.06.006
[39] Zhang Y, Yan H, Luo Y, et al. Simulation-based optimization of timetables coordination in an urban rail transit network. Simul Modell Pract Theory. 2024;130:102857. doi: 10.1016/j.simpat.2023.102857
[40] Lei Y, Lu G, Zhang H, et al. Optimizing total passenger waiting time in an urban rail network: a passenger flow guidance strategy based on a multi-agent simulation approach. Simul Modell Pract Theory. 2022;117:102510. doi: 10.1016/j.simpat.2022.102510
[41] Liao Z, Li H, Miao J, et al. Railway capacity estimation considering vehicle circulation: integrated timetable and vehicles scheduling on hybrid time-space networks. Transp Res Part C: Emerging Technol. 2021;124:102961. doi: 10.1016/j.trc.2020.102961
[42] Goverde RM, Corman F, D'Ariano A. Railway line capacity consumption of different railway signalling systems under scheduled and disturbed conditions. J Rail Transp Plann Manag. 2013;3(3):78–94. doi: 10.1016/j.jrtpm.2013.12.001
[43] Wang R, Nie L, Tan Y. Evaluating line capacity with an analytical UIC code 406 compression method and blocking time stairway. Energies. 2020;13(7):1853. doi: 10.3390/en13071853

Appendices

Appendix A. Phase-wise formulations of running time

This appendix presents the complete closed-form expressions for computing the running time $T_{i,j}^{\text{pass}}$ and the output speed $v_{i,j}^{\text{out}}$ under seven distinct operating conditions derived from the acceleration control rule in Equation (5).

- **Phase 1: Departure from origin station**

At this phase, the total distance travelled is $L_j^{\text{total}} = 0$ and the initial speed $v_{i,j}^{\text{in}} = 0$. As operations during this phase are confined to the station area, the train initially accelerates to the maximum permitted station speed and subsequently maintains this speed.

$$T_{i,j}^{\text{pass}} = (n_i - 1)t_{\text{couple}} + T_{\text{stop}} + \begin{cases} \frac{v_{\text{sta}}}{a_{\text{tra}}} + \frac{l_j - \frac{v_{\text{sta}}^2}{2a_{\text{bra}}}}{v_{\text{sta}}}, & l_j \geq \frac{v_{\text{sta}}^2}{2a_{\text{bra}}}, \\ \frac{\sqrt{2a_{\text{tra}} l_j}}{a_{\text{tra}}}, & \text{otherwise.} \end{cases} \tag{A1}$$

$$v_{i,j}^{\text{out}} = \begin{cases} v_{\text{sta}}, & l_j \geq \frac{v_{\text{sta}}^2}{2a_{\text{bra}}}, \\ \sqrt{2a_{\text{tra}} l_j}, & \text{otherwise.} \end{cases} \tag{A2}$$

- **Phase 2: Acceleration to cruising speed**

With $v_{i,j}^{\text{in}} = v_{\text{sta}}$ and $L_j^{\text{total}} + l_j < L_{\text{sta}}^k$, the pods accelerate from station limits. If the distance allows, the cruise speed v_i^{cru} is reached; otherwise, they travel at the maximum attainable speed.

- **Phase 3: Steady-state cruising**

When $v_{i,j}^{\text{in}} = v_i^{\text{cru}}$, the platoon moves at a constant cruising speed:

$$T_{i,j}^{\text{pass}} = \frac{l_j}{v_i^{\text{cru}}}, \qquad v_{i,j}^{\text{out}} = v_i^{\text{cru}}. \tag{A3}$$

- **Phase 4: Pre-station deceleration**

If $L_j^{\text{total}} + l_j \geq L_{\text{station}}$ and $L_j^{\text{total}} < L_{\text{station}}$, the train decelerates to the station speed v_{sta}:

$$T_{i,j}^{\text{pass}} = \begin{cases} \frac{v_{i,j}^{\text{in}} - v_{\text{sta}}}{a_{\text{bra}}} + \frac{l_j - \frac{\left(v_{i,j}^{\text{in}}\right)^2 - v_{\text{sta}}^2}{2a_{\text{bra}}}}{v_{\text{sta}}}, & \frac{\left(v_{i,j}^{\text{in}}\right)^2 - v_{\text{sta}}^2}{2a_{\text{bra}}} \leq l_j, \\ \frac{v_{i,j}^{\text{in}} - \sqrt{\left(v_{i,j}^{\text{in}}\right)^2 - 2a_{\text{bra}} l_j}}{a_{\text{bra}}}, & \text{otherwise.} \end{cases} \tag{A4}$$

$$v_{i,j}^{\text{out}} = \begin{cases} v_{\text{sta}}, & \frac{\left(v_{i,j}^{\text{in}}\right)^2 - v_{\text{sta}}^2}{2a_{\text{bra}}} \le l_j, \\ \sqrt{\left(v_{i,j}^{\text{in}}\right)^2 - 2a_{\text{bra}}\, l_j}, & \text{otherwise.} \end{cases} \tag{A5}$$

• **Phase 5: Terminal station full stop**
When $L_j^{\text{total}} \ge L_{\text{station}}$, the train decelerates to a complete stop:

$$T_{i,j}^{\text{pass}} = \begin{cases} \frac{v_{i,j}^{\text{in}}}{a_{\text{bra}}} + \frac{l_j - \frac{\left(v_{i,j}^{\text{in}}\right)^2}{2a_{\text{bra}}}}{0.1}, & \frac{\left(v_{i,j}^{\text{in}}\right)^2}{2a_{\text{bra}}} \le l_j, \\ \frac{v_{i,j}^{\text{in}} - \sqrt{\left(v_{i,j}^{\text{in}}\right)^2 - 2a_{\text{bra}}\, l_j}}{a_{\text{bra}}}, & \text{otherwise.} \end{cases} \tag{A6}$$

$$v_{i,j}^{\text{out}} = \begin{cases} 0, & \frac{\left(v_{i,j}^{\text{in}}\right)^2}{2a_{\text{bra}}} \le l_j, \\ \sqrt{\left(v_{i,j}^{\text{in}}\right)^2 - 2a_{\text{bra}} l_j}, & \text{otherwise.} \end{cases} \tag{A7}$$

• **Phase 6: Intermediate-speed transition**
For $v_{i,j}^{\text{in}} \in (v_{\text{sta}}, v_i^{\text{cru}})$, platoons either accelerate to cruise or decelerate to station limits:

$$T_{i,j}^{\text{pass}} = \begin{cases} \frac{v_i^{\text{cru}} - v_{i,j}^{\text{in}}}{a_{\text{tra}}} + \frac{l_j - \frac{\left(v_i^{\text{cru}}\right)^2 - \left(v_{i,j}^{\text{in}}\right)^2}{2a_{\text{tra}}}}{v_i^{\text{cru}}}, & \frac{\left(v_i^{\text{cru}}\right)^2 - \left(v_{i,j}^{\text{in}}\right)^2}{2a_{\text{tra}}} \le l_j, \\ \frac{v_{i,j}^{\text{in}} - \sqrt{\left(v_{i,j}^{\text{in}}\right)^2 - 2a_{\text{bra}}\, l_j}}{a_{\text{bra}}}, & \text{otherwise.} \end{cases} \tag{A8}$$

$$v_{i,j}^{\text{out}} = \begin{cases} v_i^{\text{cru}}, & \frac{\left(v_i^{\text{cru}}\right)^2 - \left(v_{i,j}^{\text{in}}\right)^2}{2a_{\text{tra}}} \le l_j, \\ \sqrt{\left(v_{i,j}^{\text{in}}\right)^2 - 2a_{\text{bra}}\, l_j}, & \text{otherwise.} \end{cases} \tag{A9}$$

• **Phase 7: Overspeed state**
If $v_{i,j}^{\text{in}} > v_i^{\text{cru}}$, a constant-speed approximation is applied:

$$T_{i,j}^{\text{pass}} = \frac{l_j}{\max\left(|v_{i,j}^{\text{in}}|, 0.1\right)}, \qquad v_{i,j}^{\text{out}} = v_{i,j}^{\text{in}}, \qquad v_{i,j}^{\text{in}} = v_i^{\text{cru}}. \tag{A10}$$

Appendix B. Derivation of the Objective Function Decomposition

Based on the recursive headway constraints defined in Equation (20), where the headway between successive platoons is implicitly determined by signalling and braking rules and can be equivalently expressed as a function of the cruising speed. The entry time of the final platoon N into the first block is the sum of the start time and all preceding headways:

$$t_{N,1} = t_{1,1} + \sum_{i=1}^{N-1} h_{\text{opt}}^{(i,1)}\left(v_i^{\text{cru}}\right) \tag{B1}$$

where $h_{\text{opt}}^{(i,1)}\left(v_i^{\text{cru}}\right)$ denotes the minimum admissible time headway between platoon i and its predecessor at the first block, implicitly induced by signalling and braking constraints, and

evaluated at the cruising speed v_i^{cru}. The total infrastructure occupation time T_{pass} is defined as the time when the last platoon clears the final block M, relative to the start:

$$T_{\mathrm{pass}} = t_{N,M} - t_{1,1} = (t_{N,1} + T_{\mathrm{run}}^{(N)}) - t_{1,1} \tag{B2}$$

Substituting Equation (B1) into the expression above yields the following decomposition:

$$T_{\mathrm{pass}} \approx \sum_{i=1}^{N-1} h_{\mathrm{opt}}^{(i,1)}(v_i^{\mathrm{cru}}) + T_{\mathrm{run}}^{(N)}(v_N^{\mathrm{cru}}) \tag{B3}$$

The expression consists of two parts: the first term represents the cumulative minimum safety-induced headways generated by the preceding platoons, and the second term represents the running time of the final platoon. These two components can be examined independently. Since the headway function $h_{\mathrm{opt}}(v)$ is convex, its minimum occurs at the capacity-optimal speed v_{cap}^* defined by $\partial h/\partial v = 0$. Consequently, for the preceding platoons ($i < N$), the optimal cruise speed v_i^{cru} approaches v_{cap}^*. In contrast, the running time $T_{\mathrm{run}}(v)$ decreases monotonically with increasing speed, so the minimum of the second term is achieved at the maximum permissible speed $v_{\max}$. Therefore, for the final platoon ($i = N$), the optimal cruise speed v_N^{cru} converges to $v_{\max}$.